

SUPPLEMENTAL RESEARCH DATA

Mechanisms to suppress multipolar divisions in cancer cells with extra centrosomes

Mijung Kwon, Susana A. Godinho, Namrata S. Chandhok, Neil J. Ganem, Ammar Azioune, Manuel Thery and David Pellman

TABLE OF CONTENTS

Index of Figures.....	2
Index of Tables.....	4
Index of Movies.....	5
Supplemental Material and Methods.....	7
1. Protocols.....	7
2. Data Analysis and Statistics.....	17
References.....	19
Supplemental Figures	20
Supplemental Tables.....	33

Index of Figures

- **Figure S1:** This figure shows that S2 cells contain multiple centriole pairs that are clustered to form bipolar spindles and thus were suitable for our screen.
- **Figure S2:** This figure shows that proteasome inhibitor treatment (MG132) in S2 cells increases metaphase figures without perturbing bipolar spindle formation. These conditions were critical to increase the number of mitotic cells scored for each RNAi treatment on a genome-wide scale.
- **Figure S3:** This figure, related to Figure 1, shows the distribution of the number of spindles scored for each RNAi condition as well as the classification of positive RNAi based on a 95% CI for the primary screen.
- **Figure S4:** This figure, related to Figures 2 and 3, shows that multipolar spindles promoted by either Ncd depletion or LatA treatment have an increased number of BubR1 foci when compared with control bipolar metaphase spindles.
- **Figure S5:** This figure, related to Figure 6, shows that depolymerization of astral microtubules (MTs) induces multipolar spindles in MDA-231 cancer cells with supernumerary centrosomes.
- **Figure S6:** This figure, related to Figure 6A and 6B, shows time lapse still images of MDA-231 cells undergoing cell division by DIC. Bipolar and multipolar cell divisions can be correlated with interphase cell shape. All MDA-231 cells undergoing multipolar anaphases/telophases have extra centrosomes as shown by anti-centrin staining.
- **Figure S7:** This figure, related to Figure 6, shows that disruption of cortical heterogeneity and increased adhesion strength (also likely disrupts cortical heterogeneity) can lead to multipolar spindles.
- **Figure S8:** This figure, related to Figure 7, shows that HSET depletion in various cells induces multipolar anaphase in cells with supernumerary centrosomes.

- **Figure S9:** This figure, related to Figure 7, shows that HSET can be efficiently depleted in N1E-115 and NIH-3T3 cells.
- **Figure S10:** Model for centrosome clustering, related to Figure 6.

- **Index of Tables**

- **Table S1:** Validated genes required for centrosome clustering.
- **Table S2:** Primers used to synthesize dsRNA independently from genome-wide screen.
- **Table S3:** Delay in bipolar spindle formation and anaphase onset in S2 cells with extra centrosomes.
- **Table S4:** Characterization of centrosome clustering in 22 cell types.

Index of Movies

- **Movie S1:** Centrosome clustering in a S2 cell with >2 centrosomes; S2 cell expressing GFP-SAS-6 and mCherry-Tubulin (Figure 2C, lower panel).

This movie shows the process of bipolar spindle formation in cells with > 2 centrosomes by clustering supernumerary centrosomes. Centrosomes (labeled with a centriole marker, SAS-6) that are initially distributed along the nuclear envelope before nuclear envelope breakdown (NEBD), coalesce into two poles. In cells with more than 2 centrosomes, bipolar spindle formation is delayed, compared to cells with 2 centrosomes.
- **Movie S2:** Anaphase onset in a S2 cell with 2 centrosomes; S2 cell expressing GFP-Cid and mCherry-Tubulin.
- **Movie S3:** Anaphase onset in a S2 cell with >2 centrosomes; S2 cell expressing GFP-Cid and mCherry-Tubulin (Figure 2E). This movie shows that cells with extra centrosomes have delayed anaphase onset when compared with cells with 2 centrosomes. The normal kinetochore number indicates that these cells have not previously failed cytokinesis/undergone mitotic slippage.
- **Movie S4:** Anaphase onset in a S2 cell depleted of Mad2 with >2 centrosomes; S2 cell expressing GFP-Cid and mCherry-Tubulin after Mad2 RNAi (Figure 2E). This movie shows that the delayed anaphase observed in cells with extra centrosomes is abolished in Mad2-depleted cells and, thus, anaphase onset occurs prior to centrosome clustering and without normal chromosome congression.
- **Movie S5:** Effect of LatA treatment in centrosome clustering; S2 cell expressing GFP-SAS6 and mCherry-Tubulin (Figure 4B-c). This movie shows that centrosomes do not display cell cortex directed movement in LatA-treated cells during spindle formation.
- **Movie S6:** Centrosome clustering defect in a S2 cell depleted of Ncd; S2 cell expressing GFP-SAS6 and mCherry-Tubulin (Figure 4B-b). In contrast to the centrosome

- movements in LatA-treated cells, Ncd-depleted cells show a fast and persistent centrosome movement towards the cortex.
- **Movie S7:** Centrosome clustering defects in a S2 cell depleted of Ncd followed by LatA treatment; S2 cell expressing GFP-SAS6 and mCherry-Tubulin (Figure 4B-d). The centrosome movement towards the cell cortex observed in Ncd-depleted cells is significantly diminished after additional LatA treatment.
 - **Movie S8:** Centrosome clustering defects in a S2 cell depleted of Myo10A; S2 cell expressing GFP-SAS6 and mCherry-Tubulin after Myo10A RNAi (Figure 4C-e) Centrosome movement in Myo10-depleted cells is similar to LatA-treated cells.
 - **Movie S9:** Binucleated BSC-1 cell going through bipolar division. Positioning of the retraction fibers (RF) at two opposite sides of the mitotic cell correlates with bipolar division; DIC movie (Figure 6C)
 - **Movie S10:** Binucleated BSC-1 cell going through multipolar division. Positioning of multiple RF correlates with multipolar division; DIC movie (Figure 6C).
 - **Movie S11:** N1E-115 cells going through bipolar division after control siRNA. Despite the presence of extra centrosomes, N1E-115 cells almost always undergo bipolar divisions; DIC movie (Figure 7A)
 - **Movie S12:** N1E-115 cells going through multipolar division after HSET siRNA. Depletion of HSET induces multipolar divisions in N1E-115 cells; DIC movie (Figure 7A)

SUPPLEMENTAL MATERIAL AND METHODS

1. Protocols

RNAi screen

S2 cells were plated at a density of 1×10^4 cells/well in serum-free Schneider's medium in 384 well plates which were pre-plated with $0.25 \mu\text{g}$ dsRNA (dsRNAs are available at the *Drosophila* RNAi Screening Center, DRSC, <http://flyrnai.org>). Cells were incubated with dsRNA for 40 min at room temperature (RT) in serum free medium, followed by addition of serum-containing medium and incubated for 3.5 days to allow for protein depletion. To block the metaphase-anaphase transition, $25 \mu\text{M}$ MG132, a proteasome inhibitor, was added at the end of the RNAi treatment (3.5 day-RNAi treated cells) and incubated for an additional 9 hrs (total of ~4 day RNAi incubation). To facilitate the attachment of mitotic cells, RNAi treated cells were resuspended, transferred to new 384 well plates that were pre-coated with Concanavalin A (Con-A, 0.25 mg/ml), and the plates were spun at $1,000 \text{ rpm}$ for 1 min. Cells were fixed in 4% Paraformaldehyde (PFA) in PBS (pH 7.2), permeabilized with PBS-Triton 0.01% (PBST), incubated with 0.5% SDS in PBST, and kept in PBST at 4°C until proceeding to immunostaining. For the primary screen, fixed cells were stained for MTs and centrosomes with FITC-anti-alpha tubulin (DM1A, 1:300, Sigma) and mouse anti-gamma tubulin (GTU88, 1:500) antibodies, respectively. Alexa Fluor 568 or 594 Donkey anti-mouse IgG was used as secondary antibodies (1:1000). Cells were stained for DNA with Hoechst 33342 (1:5000, Invitrogen) in PBST and stored in same solution at 4°C .

For the primary screen, cells were imaged using an automated microscope, either the ImageXpress Micro (Molecular Devices, ICCB, inverted fully automated epifluorescent microscope, laser auto-focus, equipped with the Photometrics CoolSNAP ES digital CCD camera, MetaXpress for analysis), or the Discovery-1 (Molecular Devices, DRSC, automated filter and dichroic wheels and a six objective turret, high-speed laser auto-focus, and can measure up to eight fluorophores per assay in multi-well plates), using a 20X air objective. Auto-focusing was performed on FITC (MTs) and images were acquired from single focal plane for three channels (Hoechst, Cy3, and FITC). The secondary screen was performed in 96 well plates (1 μ g dsRNA/well for 5X10⁴cells/well) and followed almost the same methodology as the primary screen. At the end of RNAi, cells were transferred to 96 well glass-bottom plates (Whatman) for high resolution imaging. Cells were stained additionally to identify mitotic cells with anti-rabbit phospho-histone H3 and Alexa Fluor 660 Donkey anti-rabbit IgG. To ensure imaging of all centrosomes, 3D images were taken with a Zeiss Axiovert microscope and Slidebook software (Intelligent Imaging Innovations, Denver, CO) using a 40X air ELWD objective (Zeiss) with 1 μ m step size. The height (start and end point) of Z stacks were manually adjusted for all 701 RNAi conditions.

Generation of double stranded RNA (dsRNA)

Double stranded RNA (dsRNA) for the primary and secondary screens were independently generated and provided by the DRSC (<http://flyrnai.org/>). For all the genes we did follow up experiments on, dsRNA was generated in the lab with primers that were chosen to amplify non-overlapping regions of a gene (Table S2). The independent dsRNAs were generated to avoid off target (OT) effects using either bacterial clones

(*Drosophila* Genome Resource Center, DGRC, <https://dgrc.cgb.indiana.edu/>) or S2 cell cDNA library (Kulkarni et al. 2006). In brief, cDNA library was prepared using the First strand cDNA synthesis kit (Fermentas) and was subsequently used as a template for PCR. Obtained amplicons were *in vitro* transcribed using MegascriptT7 kit (Ambion) and RNA was purified with Illustra Quickprep mRNA purification kit (GE Healthsciences).

Optimization of the detection of multipolar spindles in the screen

We optimized conditions to detect multipolar spindles, transferring cells to plates coated with a low concentration of concanavalin A (Con-A), followed by immediate fixation. Of note, our conditions differ significantly from those of a recent genome-wide RNAi screen in S2 cells where strong attachment enforced a round and very flat morphology and metaphase arrest was induced for a prolonged period of time (Goshima et al. 2007).

Attachment of S2 cells to high concentration of Con-A (0.5 mg/ml) for 2-3 hrs enforces a round and very flat morphology, which is ideal for microscopic observations (Rogers et al. 2002; Goshima et al. 2007). During optimization of the screen protocol, we observed that these methods are not suitable for our screen for several reasons. We attached cells on glass or different concentrations of Con-A (0-0.5 mg/ml for 30 min-3 hrs) and quantified spindle morphology. We observed gradual increases in multipolar spindles in long term attachment of S2 cells to high concentrations of Con-A (0-0.5 mg/ml for 30-3 hrs) and dramatic increases in bipolar monastral spindles (20-30% versus ~ 55%) with a concomitant decrease in multipolar spindles when cells were attached longer. Live imaging revealed that bipolar monastral spindles can be formed via a backup mechanism; multiple centrosomes initially collapsed to one focus (monopolar spindle) and MTs were assembled and focused to form the second pole that lacks centrosomes

(Goshima and Vale 2003). Monastral bipolar spindles were formed at low frequency (<30%) in cells attached to glass or low concentration of Con-A but were formed at high frequency (~55%) in cells attached to high concentration of Con-A. Therefore, to minimize the background of multipolar spindles and the backup mechanism that could mask multipolar spindles, cells were immediately attached to 0.25 mg/ml of Con-A for 1min by centrifugation prior to fixation in our RNAi screen (Figure 1B). In follow-up experiments, S2 cells were plated on 0.1-0.25 mg/ml of Con-A for 30 min prior to fixation for immunofluorescence. For live imaging, S2 cells were attached to 0.1 mg/ml of Con-A and imaged for 3-4 hrs. This condition was used to minimize spindle artifacts.

Immunofluorescence

Immunofluorescence in S2 cells was done as described in the RNAi screen section except for the use of 0.2% PBST instead of 0.5% SDS for permeabilization. Mammalian cells were fixed in cold methanol (Sigma) at -20°C for 10 min or with 4% PFA (Sigma) in PBS for 15 min at RT. N1E-115 cells, plated on poly-D-Lysine-coated coverslips (BD Biosciences), were fixed in cold methanol at -20°C for 5 min. Cells were permeabilized with 0.2% PBST for 5 min, blocked with 5% BSA in 0.1 % PBST for 30 min, and stained for primary and secondary antibodies for 1hr. DNA was stained with Hoechst 33342 at RT. Coverslips were mounted using Moiwol mounting medium and analyzed on an Axiovert 200M inverted microscope (Zeiss). Images were acquired with a CCD camera (CoolSnap, Photometrics) and Slidebook software (Intelligent Imaging Innovations, Denver, CO). For the fibronectin (FN) experiments, MDA-231 cells were plated on FN-coated coverslips as previously described (de Rooij et al. 2005) for 16hrs prior to fixation.

Antibodies

The following antibodies were used for immunofluorescence: *Drosophila* anti-D-PLP (1:1000) provided by David Glover, anti-SAS4 (1:500) provided by Jordan Raff (Basto et al. 2006), rabbit anti-HSET (1:1000) provided by Claire Walczak, human anti-Centrin-2 (1:2000) provided by Michel Bornens (Laoukili et al. 2000), anti-BubR1 (1:3000) provided by Claudio Sunkel (Logarinho et al. 2004), human anti-Pericentrin (1:1500; Abcam), mouse monoclonal α -tubulin DM1A (1:1000; Sigma) and anti-rabbit Phospho-histone H3 (Millipore). Secondary antibodies (Alexa Fluor 488, 568, 594, 660) were purchased from Molecular probes. For immunoblots, we used mouse α -tubulin DM1A (1:2000), rabbit anti-Myo10 (1:1000) provided by Mitsuo Ikebe (Tokuo and Ikebe 2004) and rabbit anti-HSET (1:1000) provided by Claire Walczak.

Live cell imaging

S2 cells were imaged using a spinning-disc confocal system (Yokogawa) mounted on a Zeiss 200M inverted microscope equipped with a 100X 1.4 NA objective at RT. 3D time-lapse (4D) imaging was performed by acquiring images every 40 sec with an EM-CCD camera (ORCA-II-ER, Hamamatsu). Z stacks were taken with a 0.5 or 1 μ m step size. For long-term imaging, a neutral density filter was used to avoid photo-damaging cells. Long-term imaging of mammalian cells was carried out using a Nikon TE2000E inverted microscope with a cooled CCD camera (Orca II ER, Hamamatsu), an automated X-Y stage (Proscan, Prior), and the Nikon Perfect Focus System. The microscope was equipped with a climate-controlled chamber that maintained the cells at 37°C with 5% CO₂ humidified atmosphere. Images were acquired at multiple locations on the coverslip

using either a 20X or 40X Nikon Plan Fluor objectives. DIC images were acquired every 3-10 min for 18-96 hrs using Nikon NIS-Elements software.

Centrosome tracking

Centrosome tracking was performed on 4D images using Slidebook software. GFP-SAS-6 positive centriole dots were manually identified at NEBD and followed using a particle tracking module.

Cell culture and transfections

Drosophila S2 cells (Invitrogen) were cultured in Schneider medium (Invitrogen) with 10% FBS (JRH Biosciences) and penicillin, streptomycin (Invitrogen). MDA-231 cells were cultured in McCoys medium (Invitrogen) supplemented with 10% FBS (Foundation), penicillin, streptomycin, and L-glutamine (Invitrogen). MCF-7, N1E-115, BSC-1, NIH-3T3, BJ and HeLa cells were cultured in DMEM+glutamax (Invitrogen) supplemented with 10% FBS, penicillin and streptomycin. P53^{-/-} 4N MMECs derived from tumors, tMMEC, were grown in DMEM-F12 (Invitrogen) supplemented with 2% FBS, penicillin, streptomycin, fungizone, 5 ng/ml EGF (Sigma) and 10 µg/ml of insulin (Invitrogen). BT-549 and NHO2A cells were cultured in RPMI1640 medium supplemented with 10% FBS, penicillin and streptomycin. All mammalian cell lines were cultured at 37°C in a 5% CO₂ incubator.

For S2 cells, EGFP-SAS-6 under pMT promoter, EGFP-Cid under original promoter and mCherry α -tubulin under the pAc promoter were obtained from G. Rogers, S. Henikoff and G. Goshima. S2 cells were transfected with the plasmids using Cellfectin (Invitrogen). 300µg/ml of Hygromycin and 500µM of CuSO₄ were used for selecting

stably transfected cells and inducing protein expression from pMT promoter. Induction of GFP-SAS-6 was performed for short periods of time (2-4 hrs) to avoid an increase in overduplication of centrioles upon prolonged SAS-6 induction (Rodrigues-Martins et al. 2007). GFP-SAS-6 signals were apparent after 2h induction with 500 μ M CuSO₄. For siRNA, mammalian cells were transfected with Lipofectamine RNAiMAX (Invitrogen).

Drug treatment

S2 cells were treated with 40 μ M Latrunculin A (LatA, Molecular Probes) and 20 μ M Cytochalasin D (Sigma) for 2 hrs to disrupt the actin cytoskeleton. Mammalian cells were treated with 5 μ M of LatA, 10 μ M of Dihydrocytochalasin B (DCB, Sigma) for 2 hrs. 10-20nM of Nocodazole (Sigma) was used for 3hrs to depolymerize astral MTs. Src kinase inhibitor, PP2 (Calbiochem), was used at 20, 40 and 50mM for 3 hrs. Calyculin A (CA, Sigma, 0.75nM in S2 cells and 0.1 nM in mammalian cells) was added to cells for 3 hrs prior to fixation. Con-A (Sigma, 0.25 mg/ml for S2 and 0.5mg/ml for mammalian cells) was added to the medium for 3-4 hrs. Tetraploid BSC-1, BJ and NIH-3T3 cells were generated by treatment with 4 μ M DCB (20 hrs) followed by release into drug-free medium.

Generation of EGFP-centrin plasmids

For EGFP-centrin constructs, blast search with human centrin 2 and 1 identified two possible *Drosophila* centrans (CG17493 and CG31802). Amino acid percent identity by Clustal W. analysis revealed that CG17493 is the closest homologue to human and mouse centrin 2 (~70 % identity) and CG31802 is second closest (~60% identity), suggesting that *Drosophila* has two centrans. The putative centrin homologues were PCR

amplified and cloned into the *Drosophila* expression vector pMT/V5-His (Invitrogen). This produced a N-terminal fusion protein of centrin and mRFP under the control of the copper-inducible promoter, pMT.

Quantitation of BubR1 foci

For the quantitation of BubR1 foci, 3D images (0.5 μ m step size) were taken with same exposure and settings for all conditions. Fluorescence signal intensity of discretely stained BubR1 foci was determined by an intensity thresholding step using Slidebook software. The number of BubR1 foci in bipolar spindles in control, and multipolar spindles in Ncd-depleted (RNAi) or LatA-treated (2h) S2 cells were scored.

siRNA

Mixed pools (ON-TARGETplus SMART pools) of 4 different oligos of siRNAs against human HSET, human Myo10 and mouse Myo10 were purchased from Dharmacon. siRNA against mouse HSET was purchased from Ambion. Non-specific scrambled siRNA was used as control (Ambion). Cells were transfected with Lipofectamine RNAiMAX (Invitrogen) with a final siRNA concentration of 50nM according to the manufacturer's instructions. Cells were analyzed/harvested 3 days after transfection (unless specified).

	Oligo sequence 5'-3'	siRNA ID#
Human HSET	UAACUGACCCUUUAAGUCCUU	J-004958-06
	AGUGUUGUGCGCUCUGUCCUU	J-004958-07
	GACACAAGCACGCAAGUUCUU	J-004958-08
	UGGUCCAACGUUUGAGUCCUU	J-004958-09
Human Myo10	CAAGUUGAGAUUUAUGUCCUU	J-007217-05
	UAAGACAUCAGCUACGACGUU	J-007217-06
	UAAUCUACAAUUCUCCCGCUU	J-007217-07
	AUUCCUGAAAUUUCCUCCUU	J-007217-08
Mouse HSET	GGCUAAUAAGAAGUGAAGtt	287750
	GGAACUGAAGGGCAAUAUCtt	287751
	GGCCAUUACAGCAGUCUGtt	287752
Mouse Myo10	UUCCACGGUGCCCUUGAGCUU	J-062004-09
	UUCUCCUCGCUAUCGUUUUUU	J-062004-10
	UUUCUUGUGCAGCCAGCCUUU	J-062004-11
	UACAUCAGCUUCGACUGGCUU	J-062004-12

Fibronectin (FN) micro-patterns

Glass coverslips were first washed with ethanol and dried before being coated with a polystyrene layer. Coverslips were manually dipped for 30 seconds in a 0.5% polystyrene solution in toluene and dried by solvent evaporation at RT. The polystyrene layer was firmly attached to the glass by UV irradiation using a mercury lamp (Heraeus Noblelight GmbH, Germany, NNQ lamp, $\lambda = 185$ nm, quartz tube, 60 W) at 10 cm distance for 5 min. Polystyrene coated glass coverslips were stored for several days in a closed chamber. The polystyrene layer was then oxydized with plasma oxygen treatment (Harrick Plasma, Ithaca, NY) for 10 seconds with a power of 30W just before the microprinting step.

Microstructured stamps were made as previously described (They et al. 2006). Briefly, molds for the stamps were produced with classical UV lithography technique by illuminating a positive photoresist through a chrome photomask on which micropatterns were designed with an electron beam. Polydimethylsiloxane (PDMS) (Sylgard 184 kit, Dow Corning) was cast on the resist mold using a 10:1 ratio (w/w) of elastomer to hardener and cured 3 hrs at 60°C. The 4 mm-thick cross-linked PDMS layer was peeled-off and stamps were manually cut out of it.

The PDMS stamp was inked with a 50 µg/ml FN solution (Sigma) 10% of which was labelled with Cy3 (Amersham Biosciences) for 30 minutes. After complete aspiration of the FN solution, the stamp was dried under the hood and placed in contact with the polystyrene coated glass coverslip for 2 minutes. After removal of the stamp, the printed coverslip was immersed in a 0.1 mg/ml solution of poly-L-lysine-g-poly ethylene glycol (PLL(20)-g[3.5]-PEG, SurfaceSolutions) in PBS to backfill non-printed areas and prevent cell adhesion around the micropatterns. The coverslip was then washed twice in PBS, dried under the hood and stored in an argon atmosphere for several days.

Colony formation assays

N1E-115 cells were plated at 10^3 per well in 6-well plates. Cells were stained with crystal violet and images were acquired using a Multi-image light cabinet (Alpha Innotech IS5500) and analyzed AlphaEase FC software.

2. Data Analysis and Statistics

Quantitation of centrosome clustering defects/multipolar spindles

Approximately, 150 cells/well and an average of 51.9 mitotic spindles/ RNAi condition were analyzed in primary screen (Figure S3A). For the secondary screen, 292 genes among 701 genes identified from primary screen were re-tested. Multipolar spindles were quantified from ~200 mitotic spindles/RNAi conditions.

For the secondary screen and further analysis of the genes of interest, spindle phenotypes were scored systematically into 6 categories due to the complex nature of spindle morphology in S2 cells; monopolar, bipolar (bipolar with 2 gamma tubulin foci), bipolar monastral (bipolar with 1 gamma tubulin focus at one pole), bipolar with scattered centrosomes, large multipolar and multiasters. Multiasters appear to be a less severe phenotype than multipolar spindles. They are more frequently observed in cells treated with actin drugs, reflecting the lack of pulling forces on centrosomes by astral MT-cortical interaction. In S2 cells, we defined centrosome clustering defects as bipolar spindles with scattered centrosomes, multipolar spindles and multiasters.

Definition of screen hits

To define the primary and secondary screen hits we calculated a Phenotypic Score (PS), which equals $\log_2(100-\text{exp}/100-\text{ctr})$, where exp is the observed value of each RNAi condition and ctr is the mean value of the negative controls. A confidence Interval (CI) was defined according to the PS of the negative control (each 384 or 96 well plate contains multiple internal negative controls, dsRNA against EGFP). 95% CI from 61 negative controls (primary screen) and from 20 negative controls (secondary screen),

calculated according to t-distribution, was used to define the cut-off of the screen hits; only genes whose PS is >95% were considered.

Data presentation and statistics

All the results presented in graphics are reported as mean \pm SD unless otherwise noted. Comparisons between continuous variables were performed using an unpaired two-sided *t* test. All statistics and graphics were generated using Prism or Microsoft Excel software.

SUPPLEMENTAL REFERENCES

- Bakal, C., Aach, J., Church, G., and Perrimon, N. (2007). Quantitative morphological signatures define local signaling networks regulating cell morphology. *Science* **316** (5832): 1753-1756.
- Basto, R., Lau, J., Vinogradova, T., Gardiol, A., Woods, C.G., Khodjakov, A., and Raff, J.W. 2006. Flies without centrioles. *Cell* **125**(7): 1375-1386.
- de Rooij, J., Kerstens, A., Danuser, G., Schwartz, M.A., and Waterman-Storer, C.M. 2005. Integrin-dependent actomyosin contraction regulates epithelial cell scattering. *J Cell Biol* **171**(1): 153-164.
- Duensing, A., Liu, Y., Perdreau, S. A., Kleylein-Sohn, J., Nigg, E. A., and Duensing, S. (2007). Centriole overduplication through the concurrent formation of multiple daughter centrioles at single maternal templates. *Oncogene* **26** (43): 6280-6288.
- Goshima, G. and Vale, R.D. 2003. The roles of microtubule-based motor proteins in mitosis: comprehensive RNAi analysis in the Drosophila S2 cell line. *J Cell Biol* **162**(6): 1003-1016.
- Goshima, G., Wollman, R., Goodwin, S.S., Zhang, N., Scholey, J.M., Vale, R.D., and Stuurman, N. 2007. Genes required for mitotic spindle assembly in Drosophila S2 cells. *Science* **316**(5823): 417-421.
- Kiger, A. A., Baum, B., Jones, S., Jones, M. R., Coulson, A., Echeverri, C., and Perrimon, N. (2003). A functional genomic analysis of cell morphology using RNA interference. *J Biol* **4**(4): 27.
- Kulkarni, M.M., Booker, M., Silver, S.J., Friedman, A., Hong, P., Perrimon, N., and Mathey-Prevot, B. 2006. Evidence of off-target effects associated with long dsRNAs in Drosophila melanogaster cell-based assays. *Nature methods* **3**(10): 833-838.
- Laoukili, J., Perret, E., Middendorp, S., Houcine, O., Guennou, C., Marano, F., Bornens, M., and Tournier, F. 2000. Differential expression and cellular distribution of centrin isoforms during human ciliated cell differentiation in vitro. *J Cell Sci* **113** (Pt 8): 1355-1364.
- Lingle, W. L., and Salisbury, J. L. (1999). Altered centrosome structure is associated with abnormal mitoses in human breast tumors. *Am J Pathol* **155** (6): 1941-1951.
- Logarinho, E., Bousbaa, H., Dias, J.M., Lopes, C., Amorim, I., Antunes-Martins, A., and Sunkel, C.E. 2004. Different spindle checkpoint proteins monitor microtubule attachment and tension at kinetochores in Drosophila cells. *J Cell Sci* **117**(Pt 9): 1757-1771.
- Rodrigues-Martins, A., Bettencourt-Dias, M., Riparbelli, M., Ferreira, C., Ferreira, I., Callaini, G., and Glover, D.M. 2007. DSAS-6 organizes a tube-like centriole precursor, and its absence suggests modularity in centriole assembly. *Curr Biol* **17**(17): 1465-1472.
- Rogers, S.L., Rogers, G.C., Sharp, D.J., and Vale, R.D. 2002. Drosophila EB1 is important for proper assembly, dynamics, and positioning of the mitotic spindle. *J Cell Biol* **158**(5): 873-884.
- Somma, M.P., Fasulo, B., Siriaco, G., and Cenci, G. 2003. Chromosome condensation defects in barren RNA-interfered Drosophila cells. *Genetics* **165**(3): 1607-1611.
- Thery, M., Jimenez-Dalmaroni, A., Racine, V., Bornens, M., and Julicher, F. 2007. Experimental and theoretical study of mitotic spindle orientation. *Nature* **447**(7143): 493-496.
- Thery, M., Pepin, A., Dressaire, E., Chen, Y., and Bornens, M. 2006. Cell distribution of stress fibres in response to the geometry of the adhesive environment. *Cell Motil Cytoskeleton* **63**(6): 341-355.
- Tokuo, H. and Ikebe, M. 2004. Myosin X transports Mena/VASP to the tip of filopodia. *Biochemical and biophysical research communications* **319**(1): 214-220.

SUPPLEMENTAL FIGURES

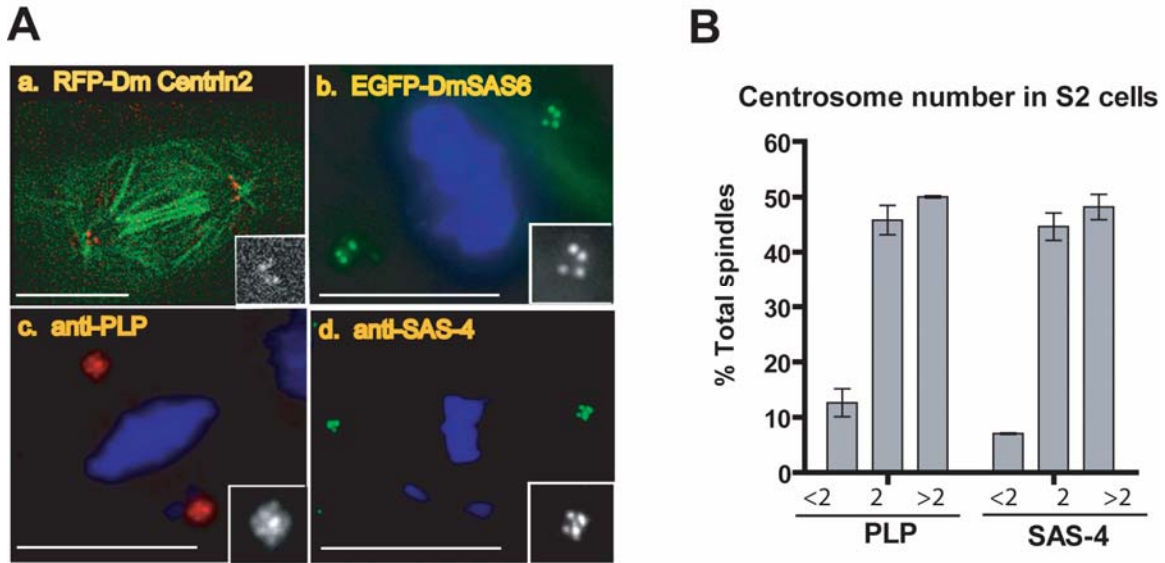


Figure S1. S2 cells contain multiple centriole pairs that are clustered to form bipolar spindles. S2 cells contain a genuine increase in the number of centrosomes, evidenced by detection with four independent centriole markers, but cluster extra centrosomes efficiently to form a bipolar spindle. The occurrence of multipolar spindles was rarely observed (~3%). **A.** High magnification images show that S2 cells contain multiple centrioles detected by (a) RFP-Dm centrin2, (b) EGFP-Dm SAS-6, (c) anti-D-PLP (Pericentrin-like protein) and (d) anti-Dm SAS-4. Inset shows high magnification of the spindle poles containing multiple centrioles. **B.** Quantitation of the number of centrosomes in mitosis as judged by anti-D-PLP or anti-SAS-4 revealed that ~50% of cells have extra centrosomes (> 2 pairs of centrioles during mitosis). All γ -tubulin foci correspond to one or more centriole pair as shown by SAS-4 or PLP co-staining (data not shown). Graph shows the average of two independent experiments (mean \pm SD). Scale bar=10 μ m.

Supplemental Note to Figure S1: Characterization of different Drosophila cells

8 *Drosophila* cell lines (S2, Sc*, S2R+, S2C, Kc, DL2, SL2, S3, gifts from DRSC) were examined to identify an ideal cell line to perform the genome wide screen. To check the robustness of centrosome clustering, we generated double-ploid cells and examine their viability as well as centrosome organization during mitoses. We were able to establish stably growing double-ploid S2 and Sc* cultures: double-ploid S2R+, S2C, Kc, SL2, S3 cells failed to maintained their ploidy status and SL2 did not produce 8C peak (G₂/M peak of double-ploid cells). Isolated double-ploid cultures of S2 and Sc* cells by FACS sorting maintain the ploidy status for several months *in vitro*, as judged by FACS. Both wild type S2 and Sc* cells have 4N DNA content whereas corresponding double-ploid cells have 8N content by metaphase chromosome spreads [data not shown, (Somma et al. 2003)]. In both S2 and Sc* cells, centrosome abnormalities such as detached centrosomes and PCM fragmentation are rare. Since several genome-wide screens have previously been conducted and data are widely available in S2 cells, and 8N S2 cells efficiently undergo bipolar mitoses (data not shown), we decided to use wild type S2 cells for further study.

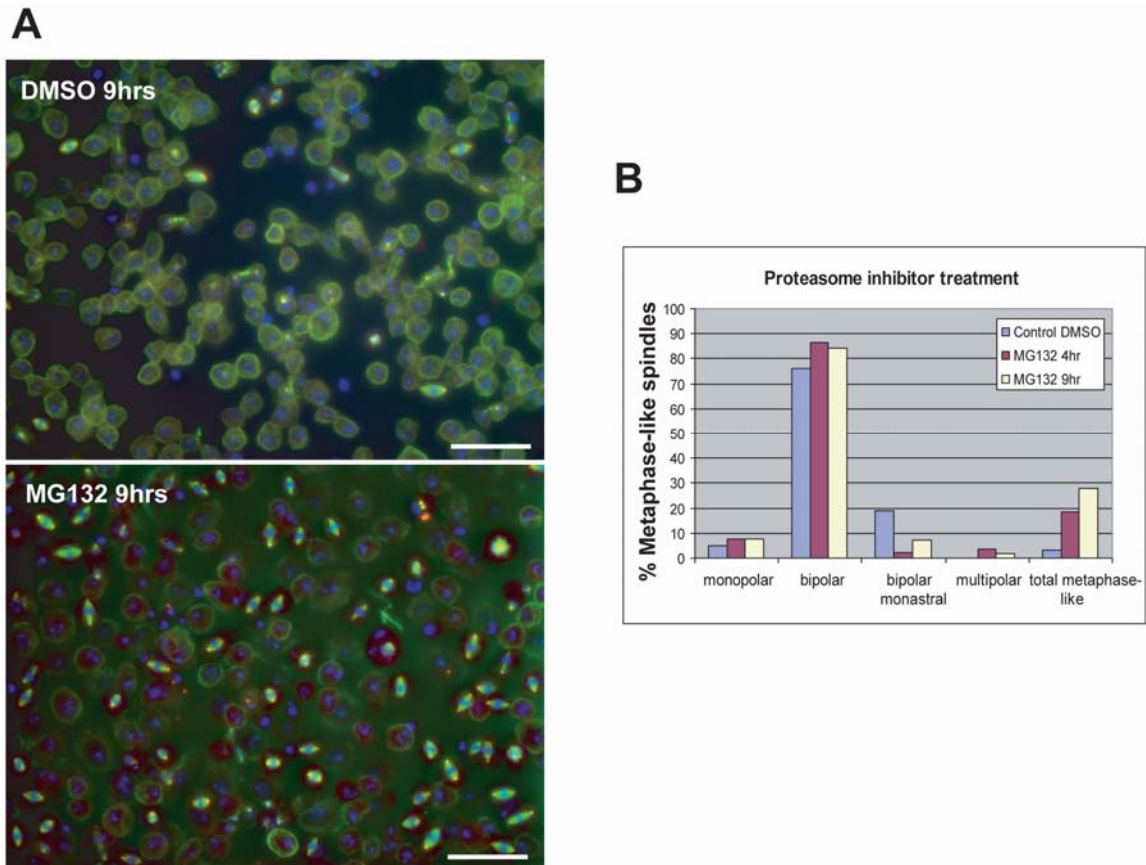


Figure S2. Proteasome inhibitor, MG132, treatment in S2 cells increases metaphase figures without perturbing bipolar spindle formation. MG132 treatment for up to 9 hrs increased the number of metaphase-like spindles (~28%) without compromising spindle bipolarity. **A.** Cells treated with DMSO or MG132 (25 μ M) for 9 hrs and stained for MTs (α -tubulin, green), centrosomes (γ -tubulin, red) and DNA (blue). **B.** Quantitation of spindle morphology after exposure to MG132 (25 μ M) or DMSO. Scale bar=50 μ m.

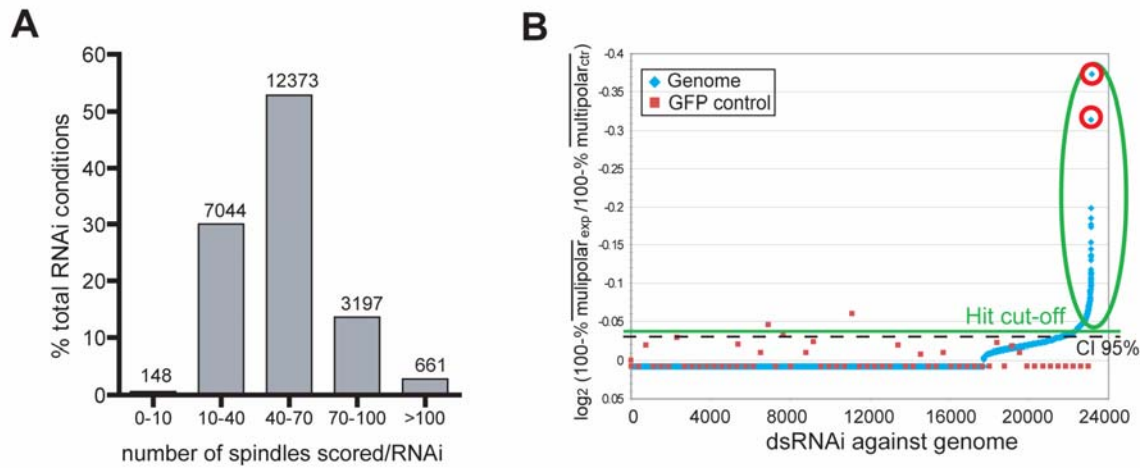


Figure S3. Genome-wide RNAi screen in S2 cells. **A.** Distribution of the numbers of metaphase spindles analyzed in each RNAi condition in the primary screen. **B.** Spindle multipolarity scored after ~24,000 dsRNAi covering 99% of the *Drosophila* genome (blue dots). A 95% confidence interval (CI, black dotted line) was generated from 61 negative controls (GFP, red dots) to define the primary hits (green circle). Red circles indicate Ncd RNAi, our strongest hit.

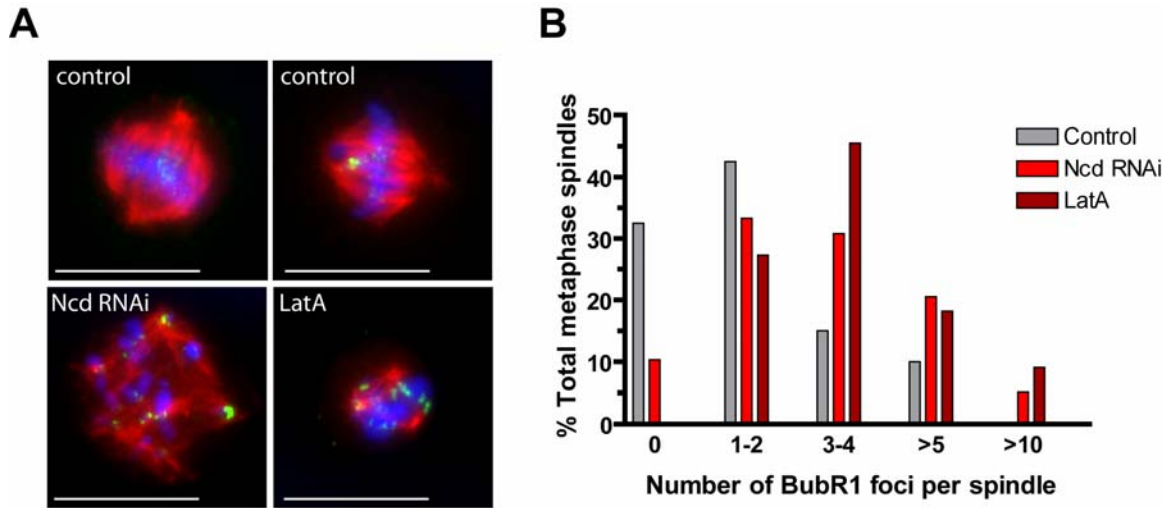


Figure S4. Increase in BubR1 localization in the multipolar spindles. An increase in the frequency of strong BubR1 foci can be observed in multipolar spindles after Ncd-depletion or LatA treatment when compared with bipolar spindles in control cells. **A.** S2 cells were stained for MTs (α -tubulin, red), BubR1 (green) and DNA (blue). **B.** Quantitation of BubR1 foci in mitotic spindles in control, Ncd-depleted and LatA-treated S2 cells. Scale bar=10 μ m.

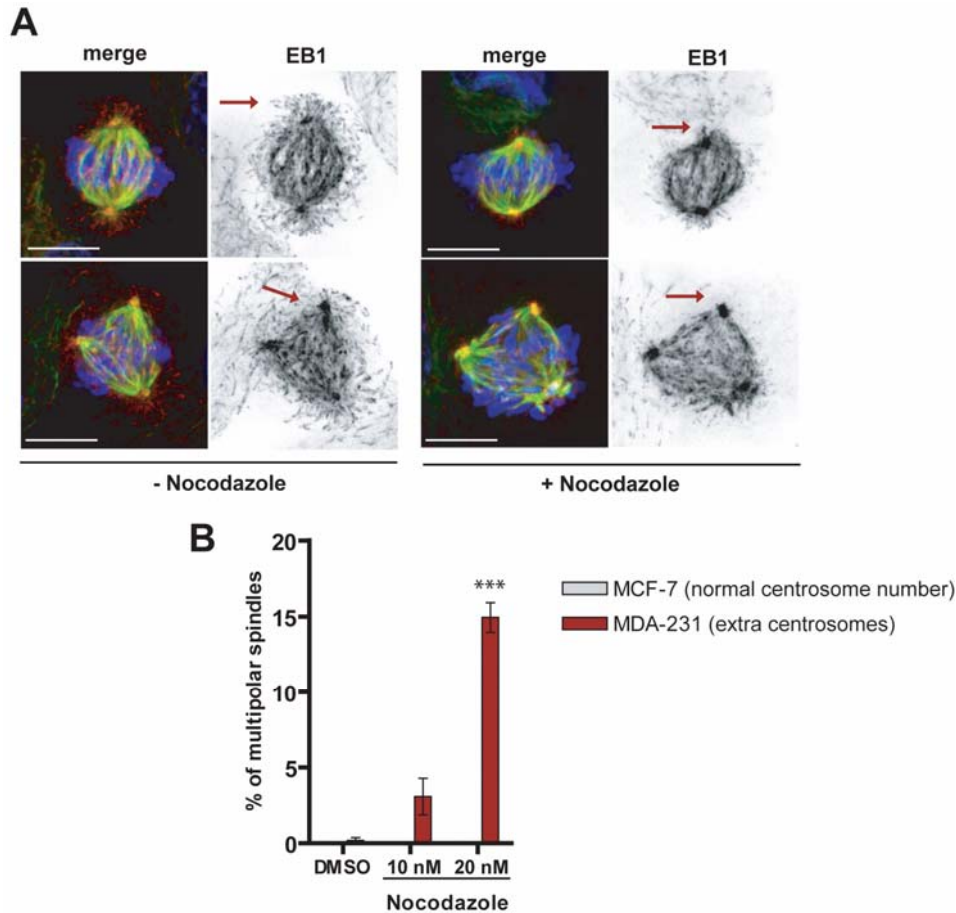


Figure S5. Astral MTs are important for suppressing multipolar mitosis only in cells with extra centrosomes. **A.** MDA-231 that contain extra centrosomes cells were stained for MTs (α -tubulin, green), EB1 (red) and DNA (blue) before and after low-dose nocodazole treatment (10-20nM for 3hrs). Red arrows point to regions where astral MTs normally localize. **B.** Quantitation of multipolar spindles after treatment with DMSO or low doses of nocodazole to depolymerize astral MTs in MCF-7 and MDA-231 cells (loss of astral MTs verified by the MT (+) tip binding protein EB1). The percentages shown are the average of three independent experiments. The percentage of multipolar spindles in MCF-7 cells is approximately zero. Graph shows the average of three independent experiments (mean \pm SD, *** p <0.001, Student's t test). Scale bar=10 μ m.

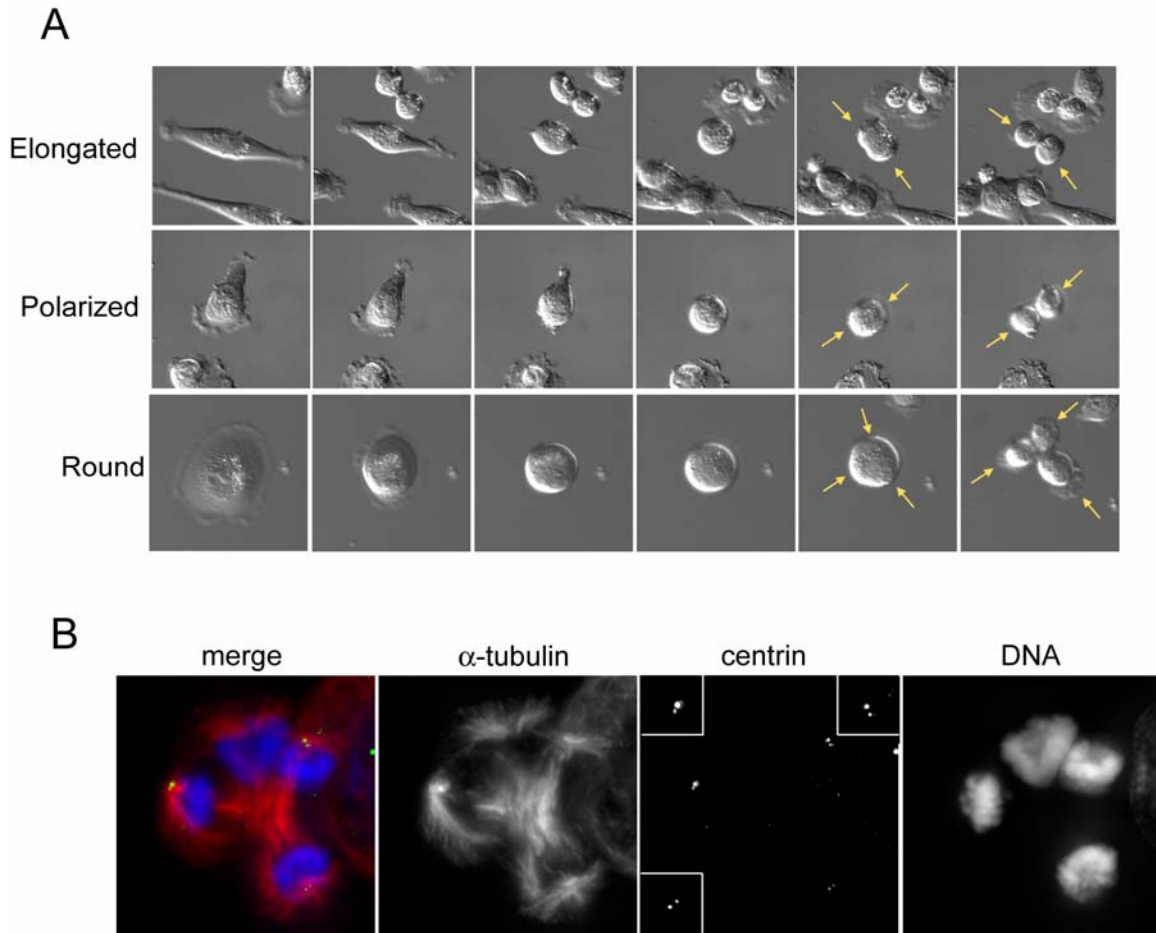


Figure S6. Bipolar and Multipolar division is correlated with interphase cell shape.

A. Still images from DIC live cell imaging of MDA-231 cells. Interphase cells with round cell shape undergo multipolar mitosis with higher frequency than elongated or polarized cells. Yellow arrows point towards the sites where daughter cells will form. **B.** MDA-231 cells that undergo multipolar telophase contain extra centrosomes. Cells were stained for MTs (α -tubulin, red), centrin (green) and DNA (blue).

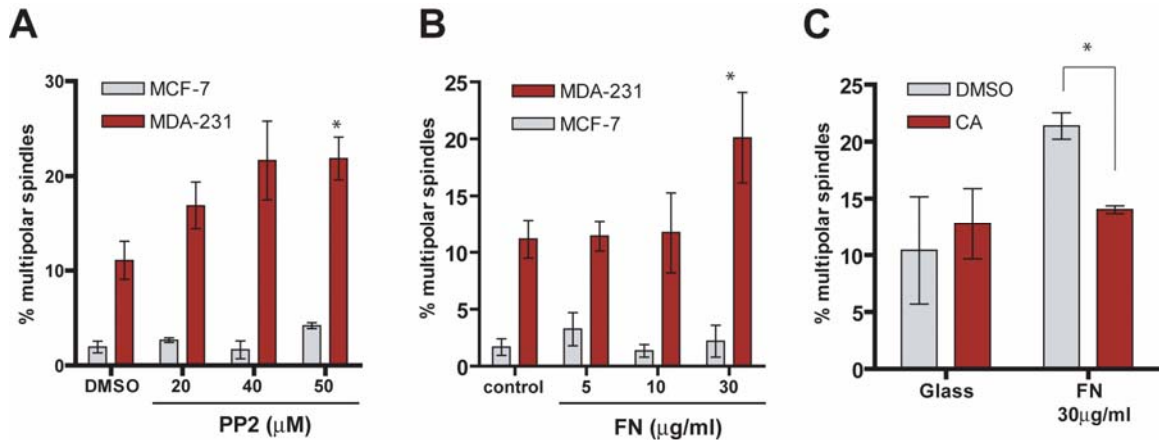


Figure S7. Cell adhesion and cortical heterogeneity are important for centrosome clustering. **A.** Quantitation of multipolar spindles in MDA-231(extra centrosomes) and MCF-7 (~normal centrosomes) cells treated with DMSO or increasing concentrations of the Src inhibitor, PP2, for 3hrs. **B.** Quantitation of multipolar spindles in MDA-231 and MCF-7 cells plated on different concentrations of fibronectin (FN) for 16 hrs. Strong adhesion promoted by a high concentration of FN decreases focal adhesion (FA) turnover. This is expected to compromise cortical heterogeneity and thus result in multipolar spindles. **C.** Quantitation of multipolar spindles in MDA-231 cells plated on glass or 30μg/ml of FN-coated coverslips both with and without calyculin A (CA, 0.1nM) treatment for 3 hrs. Addition of CA can enhance myosin contractility and promote FA turnover even in conditions of strong adhesion. As predicted from this interpretation, CA partially reverses the effect of 30μg/ml of FN. Graph shows the average of three independent experiments (mean±SD, *p<0.05, Student's t test). As predicted from this interpretation, CA partially reverses the effect of 30μg/ml of FN. Graph shows the average of three independent experiments (mean±SD, *p<0.05, Student's t test).

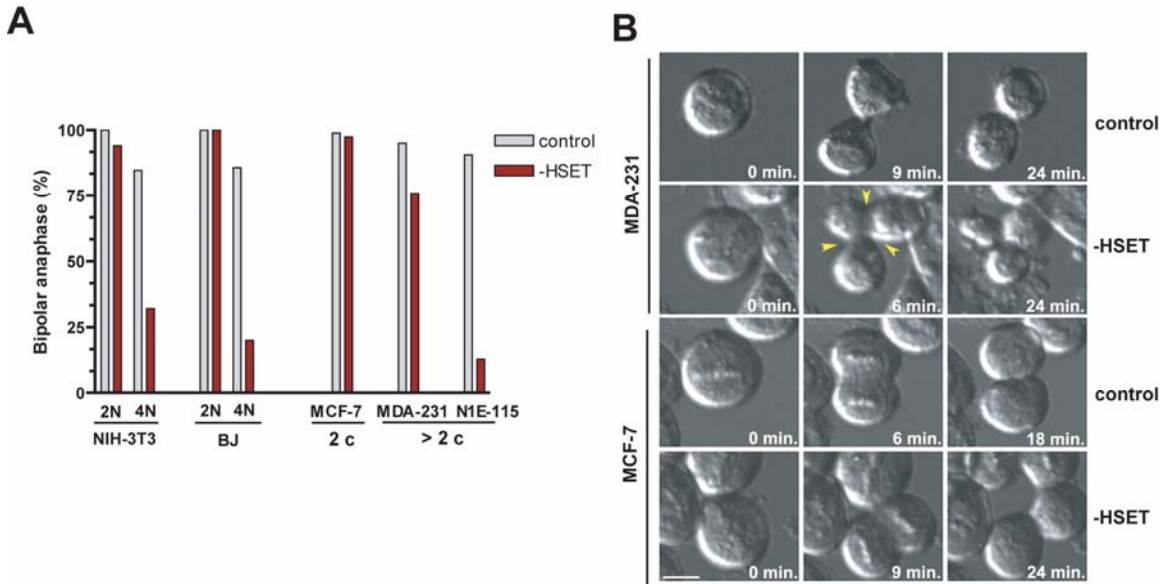


Figure S8. HSET promotes bipolar anaphase in cells with supernumerary centrosomes. A. Time-lapse imaging of cells that undergo bipolar anaphase with or without HSET depletion. Both diploid (2N, mononucleated) and isogenic tetraploid (4N, binucleated) NIH-3T3 and BJ fibroblasts, MDA-231, N1E-115 and MCF-7 cells were transfected with either scrambled siRNA (control) or HSET-specific siRNA (-HSET) and imaged throughout mitosis by DIC microscopy; 2c (2 centrosomes) and >2c (extra centrosomes) **B.** Representative DIC images from time-lapse movies of MDA-231 and MCF-7 cells treated with non-specific scrambled siRNA (control) or HSET-specific siRNA (-HSET). Yellow arrowheads indicate a tripolar anaphase. Scale bar=10μm.

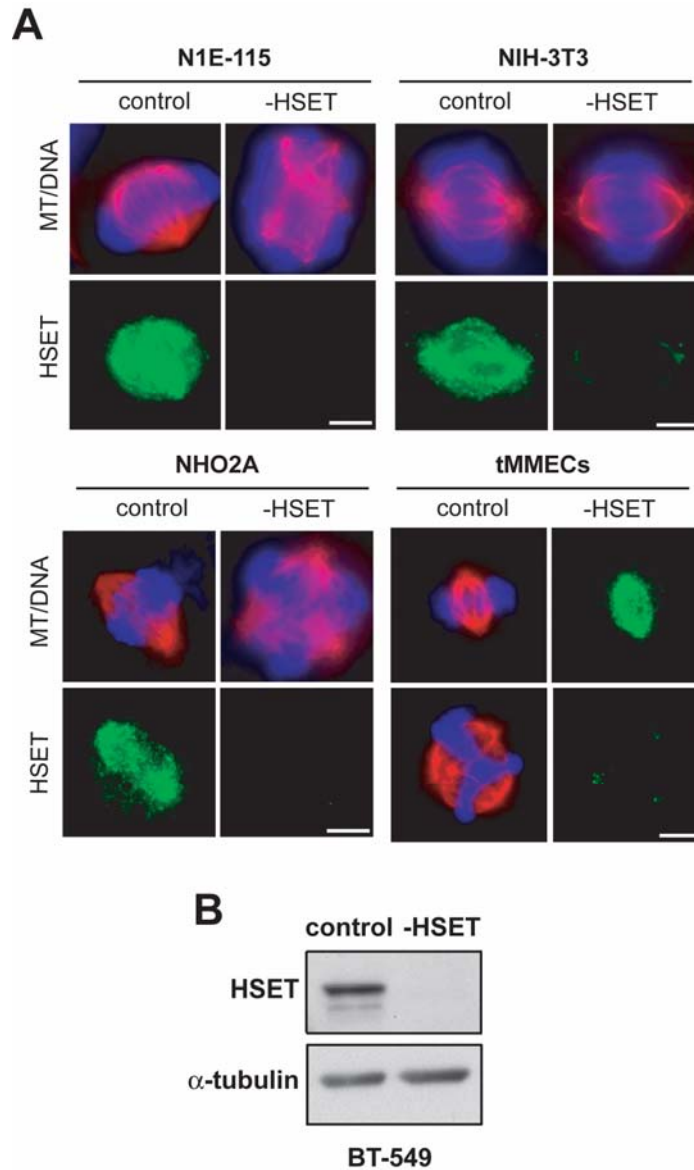


Figure S9. HSET depletion in mammalian cell lines. HSET can be efficiently depleted by siRNA in N1E-115, NIH-3T3, NHO2A, BT549 and tMMECs cells as shown by immunofluorescence (A) and western blotting (B). A. Cells transfected with control or HSET specific siRNA (-HSET) were stained for MTs (α -tubulin, red), HSET (green) and DNA (blue). Scale bar=5 μ m.

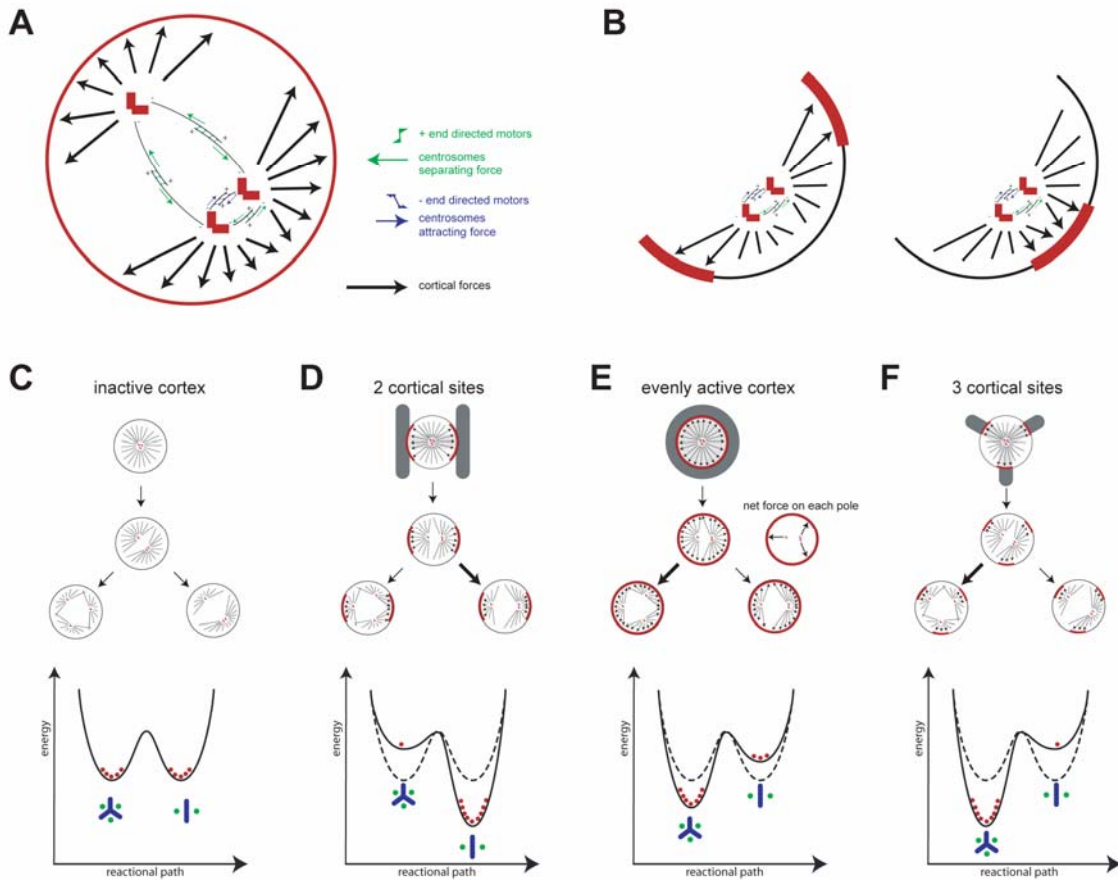


Figure S10. Model for centrosome clustering. **A.** Spindle pole separation and positioning depend on both pole-pole and pole-cortex interactions. Anti-parallel pole-pole MTs associated with plus end-directed motors (such as Eg5/Kinesin-5) promote spindle pole separation whereas minus end-directed motors (such as Ncd/HSET/Kinesin-14) promote clustering. HSET can also generate pole clustering forces within parallel MTs. In addition, the spatial distribution of pole-cortex interactions imposes additional constraints on centrosome separation via astral MTs. **B.** Specific localization of cortical cues and the corresponding distributions of forces acting on supernumerary centrosomes can either promote or prevent centrosomes separation. **C-F.**

Prediction of the energy landscape for bipolar and multipolar configuration in cells with extra centrosomes according to the distribution of cortical force generators (D-F) or when the cortex is considered inactive [no cortical force, C, (They et al. 2007)].

Supplemental Note to Figure S10: Model for centrosome clustering

It has been proposed recently that the spatial distribution of the cortical cues induce torque on astral MTs and guide spindle positioning (They et al. 2007). According to this view, spindle pole separation and spindle positioning depend on both pole-pole and pole-cortex mechanical interaction (Figure S10A). Thus, in cells containing multiple centrosomes, the specific localization of cortical cues and the corresponding distribution of forces acting on supernumerary centrosomes could either promote or prevent centrosomes separation (Figure S10B).

This simple model may explain the different proportions of multipolar spindles we measured on different micropatterns. For simplicity of discussion we will assume that bipolar and multipolar configurations are energetically equivalent in the absence of cortical forces [(although the trends do not rely on this assumption) (Figure S10C)]. When plated on H-shaped micropatterns, two cortical sites are formed in front of each bar of the H (Figure S10D). Centrosomes are attracted toward these sites and tend to cluster into groups. Centrosomes moving away from each other are pulled back together since they are attracted toward the same cortical site. Therefore the multipolar configurations, which require supernumerary centrosomes to push against each other to resist cortical attraction, correspond to a high energy state. Bipolar configurations, in which supernumerary centrosomes are clustered in front of cortical cues, correspond to a lower energy state and indeed are observed more frequently. By contrast, when cells are plated

on discoidal patterns (O pattern) cortical force generators will be distributed evenly over the entire cell periphery (Figure S10E). During the early steps of centrosomes interactions, this homogeneous distribution of tension will facilitate the separation of two close centrosomes. Multipolar configurations will correspond to a lower energy state and, as observed, will be more frequent. This effect might be exaggerated in cells plated on Y shaped micropatterns, a trend observed in our experiments (Figure S10F).

Table S1. Validated genes required for centrosome clustering

Target Gene	DRSC Amplicon	FBGN	Biological Process	Molecular Function	Off Targets	Human Homolog	Hit strength
alphaTub85E	DRSC16899	FBgn0003886	Mitosis	GTPase activity; structural molecule activity	3	TUBA1C	weak
Asp	DRSC16903	FBgn0000140	Mitosis	Microtubule binding	0	ASPM	medium
Bj1	DRSC09684	FBgn0002638	Mitosis	Ran guanyl-nucleotide exchange factor activity;chromatin binding	0	RCC1	weak
BubR1	DRSC04838	FBgn0025458	Mitosis	Serine/threonine kinase activity	0	BUB1	weak
Cid	DRSC07592	FBgn0040477	Mitosis	DNA binding	0	CENPA	strong
CLIP-190*	DRSC03283	FBgn0020503	Mitosis	Microtubule binding; actin binding; protein binding	0	CLIP-170	medium
Cmet	DRSC03511	FBgn0040232	Mitosis	Microtubule motor activity	0	CENPE	medium
Klp59C	DRSC04348	FBgn0034824	Mitosis	Microtubule motor activity	1	KIF2C/MCAK	weak
Mad2	DRSC10274	FBgn0035640	Mitosis	Protein binding	0	MAD2L1	strong
Ncd	DRSC17012	FBgn0002924	Mitosis	Microtubule motor activity	0	KIFC1/HSET	strong
Tacc	DRSC12388	FBgn0026620	Mitosis	Microtubule binding; protein binding	0	TACC	weak
Tankyrase	DRSC14154	FBgn0027508	Mitosis	Actin binding; NAD+ ADP-ribosyltransferase activity	0	TNKS	medium
Arp66B	DRSC09669	FBgn0011744	Actin cytoskeleton	Structural constituent of cytoskeleton	0	ACTR3	medium
CG5022	DRSC02802	FBgn0032225	Actin cytoskeleton	Structural constituent of cytoskeleton	0	FRMD3	medium
CG6891	DRSC20016	FBgn0030955	Actin cytoskeleton	Actin binding	0	COTL1	medium
Form3	DRSC10297	FBgn0053556	Actin cytoskeleton	Structural constituent of cytoskeleton	0	INF2	medium
Myo10A*	DRSC19834	FBgn0030252	Actin Cytoskeleton	Motor activity; structural constituent of cytoskeleton	0	MYO15	medium
Rho1	DRSC07530	FBgn0014020	Actin cytoskeleton	GTPase activity	0	RHO	strong
sced	DRSC04990	FBgn0013732	Actin cytoskeleton	Unknown	0	Dm only	medium
WASp	DRSC15032	FBgn0024273	Actin cytoskeleton	Structural constituent of cytoskeleton	0	WASL	weak
wupA	DRSC20385	FBgn0004028	Actin cytoskeleton	Structural constituent of cytoskeleton	0	Dm only	weak
Pi3K92E	DRSC16788	FBgn0015279	Signal transduction, Actin cytoskeleton	Phosphatidylinositol-4,5-bisphosphate 3-kinase activity	0	PIK3CB	medium
slik/plkk1	DRSC04471	FBgn0035001	Signal transduction, Actin cytoskeleton	Serine/threonine kinase activity	0	SLK	medium
Cad96Ca	DRSC14220	FBgn0022800	Cell adhesion	Tyrosine kinase activity	0	Dm only	weak
CG33171	DRSC11029	FBgn0053171	Cell adhesion	Extracellular matrix structural constituent	0	COL18A1	medium
ed	DRSC00478	FBgn0000547	Cell adhesion	Protein binding	0	N	weak
Fit1	DRSC08450	FBgn0035498	Cell adhesion	Cell adhesion molecule binding	1	PLEKHC1/MIG-2	medium
tutl	DRSC00441	FBgn0010473	Cell adhesion	Protein kinase activity	1	IGSF9B	medium
corn	DRSC11021	FBgn0028383	Cell polarity	Microtubule binding; protein binding	0	N	weak
crb	DRSC16927	FBgn0000368	Cell polarity	Structural molecule activity; receptor activity	0	CRB	weak
par-1	DRSC07660	FBgn0026193	Cell polarity	Serine/threonine kinase activity	0	MARK	medium
CaMKII	DRSC17214	FBgn0004624	Signal transduction	Serine/threonine kinase activity	0	CAMK2D	weak
CG31960	DRSC00281	FBgn0051960	Signal transduction	Ca/calmodulin binding	2	Dm only	weak
CG7054	DRSC16185	FBgn0038972	Signal transduction	Kinase inhibitor activity	0	Dm only	medium
Gr63a	DRSC08438	FBgn0035468	Signal transduction	G-protein coupled receptor activity	0	Dm only	strong
Gr65a	DRSC08837	FBgn0041232	Signal transduction	G-protein coupled receptor activity	0	Dm only	medium
Obp56e	DRSC07188	FBgn0034471	Signal transduction	Odorant binding	0	N	weak
Octabeta2R	DRSC16165	FBgn0038063	Signal transduction	Amine receptor activity	0	ADRB1	strong
Or47b	DRSC07492	FBgn0026385	Signal transduction	G-protein coupled receptor activity	0	N	weak
Or9a	DRSC18692	FBgn0030204	Signal transduction	G-protein coupled receptor activity	1	N	strong
Plip	DRSC14235	FBgn0039111	Signal transduction	Tyrosine/serine/threonine phosphatase activity	0	Mm Ptpm1	weak
Sdc	DRSC04654	FBgn0010415	Signal transduction	Cytoskeletal protein binding; transmembrane receptor activity	1	N	medium
spri	DRSC17985	FBgn0085443	Signal transduction	GTPase activator activity	0	RIN2	strong
stet	DRSC08283	FBgn0020248	Signal transduction	Serine-type peptidase activity; receptor signaling protein activity	0	RHBDL3	medium
unc-5	DRSC05545	FBgn0034013	Signal transduction	Netrin receptor activity	0	UNC5B	strong
upd3	DRSC19968	FBgn0053542	Signal transduction	Cytokine activity	0	N	medium
CG13630	DRSC14631	FBgn0039219	Proteolysis and Ubiquitination	Methionyl aminopeptidase activity	0	METAP1	weak
CG14869	DRSC15966	FBgn0038341	Proteolysis and Ubiquitination	Metalloendopeptidase activity	0	Dm only	strong
CG30421	DRSC04426	FBgn0050421	Proteolysis and Ubiquitination	Ubiquitin-specific protease activity	0	USP31	weak
CG5798	DRSC15876	FBgn0038862	Proteolysis and Ubiquitination	Cysteine-type endopeptidase activity	0	USP8	strong
CG9932	DRSC03275	FBgn0032469	Proteolysis and Ubiquitination	Metallopeptidase activity; nucleic acid binding	0	N	medium

Target Gene	DRSC Amplicon	FBGN	Biological Process	Molecular Function	Off Targets	Human Homolog	Hit strength
Gbp	DRSC07434	FBgn0013969	Proteolysis and Ubiquitination	Ubiquitin-protein ligase activity	1	PRPF19	weak
hiw	DRSC20338	FBgn0030600	Proteolysis and Ubiquitination	Ubiquitin-protein ligase activity	6	MYCBP2	weak
Mmp2	DRSC22024	FBgn0033438	Proteolysis and Ubiquitination	Metalloendopeptidase activity	1	MMP17	weak
Pall	DRSC10364	FBgn0036005	Proteolysis and Ubiquitination	Unknown, Fbox protein	0	FBXO28	medium
Pros25	DRSC16798	FBgn0086134	Proteolysis and Ubiquitination	Threonine endopeptidase activity	0	PSMA2	medium
Pros28.1B	DRSC04643	FBgn0017556	Proteolysis and Ubiquitination	Threonine endopeptidase activity	0	N	strong
UbcD2	DRSC01137	FBgn0015320	Proteolysis and Ubiquitination	Ubiquitin-protein ligase activity	0	UBE2E1	medium
Ubc-E2H	DRSC18221	FBgn0029996	Proteolysis and Ubiquitination	Ubiquitin-protein ligase activity	0	UBE2H	weak
CG13900	DRSC08370	FBgn0035162	DNA replication and repair	Poly(A) binding; damaged DNA binding	0	SF3B3	strong
CG2990	DRSC18254	FBgn0030170	DNA replication and repair	ATP-dependent DNA helicase activity;	0	DNA2L	weak
CG7942	DRSC10933	FBgn0035838	DNA replication and repair	Endonuclease activity	0	DBR1	medium
hay	DRSC11354	FBgn0001179	DNA replication and repair	ATP-dependent DNA helicase activity	0	ERCC3	strong
betaCop	DRSC20312	FBgn0008635	Intracellular Transport	Protein transporter activity	0	COPB1	weak
CG11575	DRSC14329	FBgn0039879	Intracellular Transport	Transporter activity	0	N	weak
CG31213	DRSC15647	FBgn0051213	Intracellular Transport	ATPase activity	0	Dm only	medium
CG9139	DRSC08628	FBgn0035202	Intracellular Transport	Guanyl-nucleotide exchange factor activity	0	RABGEF1	medium
Ent3	DRSC09822	FBgn0036319	Intracellular Transport	Nucleoside transporter activity	0	SLC29A4	strong
Kap-alpha3	DRSC16976	FBgn0027338	Intracellular Transport	Protein transporter activity	0	KPNA4	strong
rtet	DRSC14160	FBgn0028468	Intracellular Transport	Sugar transporter activity	0	TETRAN	medium
sbr	DRSC20368	FBgn0003321	Intracellular Transport	Protein transporter activity	0	INXF1	medium
Cog7	DRSC16331	FBgn0051040	Transcription, Translation, RNA processing	Transcription factor activity;	0	COG7	medium
l(2)01424	DRSC06854	FBgn0010488	Transcription, Translation, RNA processing	Translation initiation factor activity	0	EIF4G2	weak
Rpl118	DRSC12366	FBgn0003275	Transcription, Translation, RNA processing	DNA-directed RNA polymerase activity	0	POLR2F	weak
aay	DRSC11320	FBgn0023129	Miscellaneous	Serine phosphatase activity	0	PSPH	strong
Anp	DRSC14112	FBgn0000094	Miscellaneous	Unknown	0	N	strong
Calmodulin	DRSC07354	FBgn0000253	Miscellaneous	Ca/calmodulin binding	0	calmodulin	strong
CG1017	DRSC08154	FBgn0035294	Miscellaneous	Structural molecule activity	0	MFAP1	medium
CG17187	DRSC15181	FBgn0037882	Miscellaneous	Heat shock protein binding; unfolded protein binding	0	DNAJC17	medium
CG31004	DRSC15099	FBgn0051004	Miscellaneous	Unknown	0	SUSD2	medium
CG7130	DRSC11797	FBgn0037151	Miscellaneous	Heat shock protein binding; ATPase activity	0	Dm only	weak
CG8177	DRSC10969	FBgn0036043	Miscellaneous	Inorganic anion exchanger activity	0	SLC4A3	weak
CycJ	DRSC08653	FBgn0010317	Miscellaneous	Cyclin-dependent protein kinase regulator activity	0	CCNJ	medium
egg	DRSC04119	FBgn0086908	Miscellaneous	Histone-lysine N-methyltransferase activity	0	SETDB1	medium
Hsp23	DRSC11188	FBgn0001224	Miscellaneous	Actin binding	0	N	weak
Hsp70Bb	DRSC15380	FBgn0051354	Miscellaneous	ATP binding	0	HSPA	strong
Rep3	DRSC07529	FBgn0028407	Miscellaneous	Protein binding	0	N	weak
tun	DRSC05592	FBgn0034046	Miscellaneous	Unknown	0	C8orf32	medium
CG8709	DRSC07241	FBgn0033269	Miscellaneous	Unknown	0	LPIN2	strong
CG10139	DRSC05972	FBgn0033951	Unknown	Unknown	0	N	strong
CG10151	DRSC05974	FBgn0033960	Unknown	Unknown	0	N	weak
CG10347	DRSC19352	FBgn0030342	Unknown	Unknown	0	NUDCD1	weak
CG10931	DRSC06015	FBgn0034274	Unknown	Unknown	0	WDR5	medium
CG11980	DRSC14456	FBgn0037652	Unknown	Unknown	0	C12orf10	strong
CG12391	DRSC06147	FBgn0033581	Unknown	Nucleic acid binding	0	N	strong
CG13297	DRSC09971	FBgn0035685	Unknown	Unknown	0	N	strong
CG13353	DRSC06381	FBgn0033896	Unknown	Unknown	0	N	weak
CG13565	DRSC04202	FBgn0034935	Unknown	Unknown	0	N	weak
CG13858	DRSC14708	FBgn0040585	Unknown	Unknown	0	N	medium
CG13886	DRSC08356	FBgn0035163	Unknown	Unknown	0	C7orf25	weak
CG14315	DRSC14794	FBgn0038568	Unknown	Unknown	0	N	weak
CG14651	DRSC12237	FBgn0037254	Unknown	Unknown	0	Dm only	strong
CG14977	DRSC08436	FBgn0035469	Unknown	Unknown	0	N	weak
CG1553	DRSC06556	FBgn0033224	Unknown	Unknown	0	C14orf104	weak

Target Gene	DRSC Amplicon	FBGN	Biological Process	Molecular Function	Off Targets	Human Homolog	Hit strength
CG15822	DRSC08482	FBgn0035308	Unknown	Unknown	0	SESTD1	medium
CG15876	DRSC08484	FBgn0035569	Unknown	Unknown	0	N	medium
CG15925	DRSC06597	FBgn0034129	Unknown	Unknown	0	PARP16	weak
CG1621	DRSC06604	FBgn0033182	Unknown	DNA binding	3	N	weak
CG1674	DRSC17142	FBgn0039897	Unknown	Unknown	0	N	medium
CG17390	DRSC06668	FBgn0033939	Unknown	Nucleic acid binding	0	ZNF423	medium
CG18416	DRSC06747	FBgn0034482	Unknown	Unknown	0	N	strong
CG18568	DRSC06768	FBgn0033888	Unknown	Unknown	1	N	weak
CG31163	DRSC14714	FBgn0051163	Unknown	SH3/SH2 adaptor activity	0	CXorf9	medium
CG32159	DRSC09435	FBgn0052159	Unknown	Unknown	0	Dm only	weak
CG32437	DRSC22020	FBgn0052437	Unknown	Unknown	0	N	weak
CG32645	DRSC19889	FBgn0052645	Unknown	Transferase activity	0	Dm only	strong
CG32828	DRSC02612	FBgn0052828	Unknown	Unknown	0	N	weak
CG32939	DRSC15342	FBgn0052939	Unknown	Unknown	0	N	weak
CG34339	DRSC17800	FBgn0030133	Unknown	Unknown	0	N	strong
CG3517	DRSC15492	FBgn0038706	Unknown	Unknown	0	N	medium
CG4611	DRSC10434	FBgn0035591	Unknown	Unknown	0	PTCD1	medium
CG4757	DRSC14130	FBgn0027584	Unknown	Carboxylesterase activity	0	Dm only	weak
CG5059	DRSC11761	FBgn0037007	Unknown	Unknown	0	Dm only	weak
CG5070	DRSC19932	FBgn0030824	Unknown	Unknown	0	N	weak
CG5385	DRSC02854	FBgn0032215	Unknown	Unknown	0	N	weak
CG6259	DRSC10610	FBgn0036740	Unknown	Unknown	0	CHMP5	medium
CG7006	DRSC16169	FBgn0039233	Unknown	RNA binding	0	NIP7	weak
CG7158	DRSC11806	FBgn0037116	Unknown	Unknown	0	ALS2	medium
CG9919	DRSC20219	FBgn0030742	Unknown	Unknown	0	Dm only	medium
Pde11	DRSC02460	FBgn0085370	Unknown	Unknown	0	PDE5A	weak
PPP4R2r	DRSC18695	FBgn0030208	Unknown	Phosphatase activator activity	0	PPP4R2	medium
Psf3	DRSC18216	FBgn0030196	Unknown	3'-5' DNA helicase activity	0	Dm only	strong
Sc2	DRSC08162	FBgn0035471	Unknown	Unknown	0	GPSN2	strong

Genes are classified into the pie chart (Figure 1D) according to biological process

Pi3K and Slik that belong to signal transduction and actin cytoskeleton categories were considered as actin cytoskeleton in Figure 1D.

Number of predicted off targets are determined based on 21 base pair perfect matches (Kulkarni et al., 2006)

* these genes were tested directly, not identified in primary screen

Miscellaneous includes biological processes, such as cell cycle, behavior, metabolism, protein modification and cell death

N indicates that there are no mammalian homologs

Dm only indicates that these genes are only present in *Drosophila*

Screen hits defined by 95% CI were subcategorized into strong (>3.5 SD), medium (>2.5 to 3.5 SD) and weak (>1.4 to 2.5 SD) in hit strength column. SD is standard deviation.

Table S2. Primers used to synthesize dsRNA independently from genome-wide screen

Target Gene	FBGN	Forward Primer	Reverse primer
Asp	FBgn0000140	AGGCTTACAGGAAAGCCACA	AGGCTTACAGGAAAGCCACA
Bj1	FBgn0002638	ATCTGGGCCACCAACTACTG	GACCAAAAAGATTGCGTGCT
BubR1	FBgn0025458	ATTCCGTCTGAATCTCCAGTG	GCGGTGTCTTTCCAAACAAT
Calmodulin	FBgn0000253	CAGTGGCGACTTTGATGGAT	CTCCGCTTATTTTGGCAGAT
CG15925 *	FBgn0034129	ATTCCCAAATTCCTGGAC	CAGGCGAAAGAAAGTGCTTC
CG33171	FBgn0053171	AAGGACCAAAGGGTGATTCC	ACTGCCATCCCTTGTTTACG
CLIP-190	FBgn0020503	AGGCGGAGAAGAGTGAAACA	ATGTCTCCATTGGCCTCTTG
Corn	FBgn0028383	CCTGCTGATGATGGACAATG	CTTAAGTCGCTGCCCTTGA
Crb	FBgn0000368	AACGGAACCCACTGCTATTG	CCCACACAGTCGTCATGTC
Fit1	FBgn0035498	GCCTGCGCTTCAAATACTTC	GACCTCACTGTTCCGACCAT
Form3	FBgn0053556	GAGGAGGATGACCTGATGGA	GTGGTCGTAGGCGTATTCGT
Mad2**	FBgn0035640	AGGGCTCCGCTCAGATTATT	GCCTGCGGATTCTGTATGA
Myo10A	FBgn0030252	TCTACCTGGCTCGTCGAGAT	AGCTCTGCTGCTTGAGGAAG
Myo7	FBgn0000317	CGAAGGTTTCTACGCCTGAG	GCGAGCTGCATCATTGATAA
Par-1	FBgn0026193	GAGTCGAGGTCAGGAACAGC	CAGAACGTGTCCAGCTTTGA
Pi3K92E	FBgn0015279	TAGCAGCGACTACGAGCTGA	ATCGACTTGTGGAGGTGGAC
Tankyrase	FBgn0027508	CGCCGTATAGTGCTCAACAA	TAACATCGGCTCCATTCTCC

* Small overlapping region (158 nucleotide, nt) was used due to small size of gene coding region (1080nt).

** 438nt overlapping region was used due to small gene coding region (624nt).

Table S3. Delay in bipolar spindle formation and anaphase onset in S2 cells with extra centrosomes

A. Bipolar spindle formation in S2 cells.

	GFP-SAS6/ChTub				GFP-Cid/ChTub	
	Control		LatA		Control	
	2c	>2c	2c	>2c	2c	>2c
Bipolar spindle (min)	5.3	14.7	ND	22.1	7.9	21.3
Standard deviation	1.1	6.4	ND	12.3	11.0	9.9
Number of cells observed	7	15	ND	13 ^b	12	12
Fold change	2.78		1.50 ^a		2.70	

B. Anaphase onset in S2 cells

	GFP-Cid/ChTub			
	Control		Mad2 RNAi	
	2c	>2c	2c	>2c
Anaphase onset (min)	28.7	52.1	19.7	23.4
Standard deviation	11.0	29.8	7.7	8.8
Number of cells observed	12	12	14	14
Fold change	1.82		1.18	

Statistics of the data presented in Figures 2B, 2D and 3B. The data were obtained from S2 cells expressing GFP-SAS-6 and mCherry α -tubulin or GFP-Cid and mCherry α -tubulin using time lapse spinning disc confocal microscopy. Time for bipolar spindle formation corresponds to centrosome clustering (c.c.) in extra centrosome containing cells and it was determined by time taken from NEBD to clustering of extra centrosomes (SAS-6 positive) into two opposite poles (bipolar spindle formation). Anaphase onset was determined by the time taken from NEBD to the initiation of sister chromatid (Cid positive) separation.

Fold change was determined by the ratio of values from >2c (cells with >2 centrosomes) to 2c (cells with 2 centrosomes).

^a Fold change was determined by the ratio of values from LatA to DMSO-treated cells with >2 centrosomes.

^b Among total of 15 cells observed, 13 cells were used to obtain the average time since 2 cells failed to cluster centrosomes and remained as multipolar spindles during 90 min of movies (shown in red asterisks in Figure 3B).

Table S4. Characterizaion of centrosome numbers and centrosme clustering in cancer cells

Cell line	Species	Cell type/organ	Disease	2 centrosomes (%)		>2 centrosomes (%)		
				bipolar	split	clustered	multipolar	bipolar scattered
Transformed								
N1E-115	mouse	brain	neuroblastoma	0	0	42	40	18
tMMECs	mouse	mammary gland	myoepitheliomas	49	0	24	16	11
NHO2A	mouse	brain	neuroblastoma	44	0	48	8	0
MDA-231	human	mammary gland	adenocarcinoma	55	1	35	9	0
BT-549	human	breast	ductal carcinoma	55	0	31	11	3
OS#331	mouse	bone	osteosarcoma	62	0	20	18	0
OS#136	mouse	bone	osteosarcoma	65	0	23	12	0
CF-PAC-1	human	pancreas	ductal adenocarcinoma; cystic fibrosis	69	0	17	14	0
OS#330	mouse	bone	osteosarcoma	75	0	15	10	0
U373	human	brain	glioblastoma	77	0	4	19	0
T47D	human	mammary gland	ductal carcinoma	60	18	20	2	0
UPSI:SCC114	human	oral cavity	oral squamous cell carcinomas	78	0	6	16	0
HCT-116	human	colon	colorectal carcinoma	67	0	27	6	0
MCF-7	human	mammary gland	adenocarcinoma	86	0	11	3	0
HeLa	human	epithelia	adenocarcinoma	84	5	3	7	1
U-87 MG	human	brain	glioblastoma, astrocytoma	94	0	4	2	0
HT-29	human	colon	colorectal carcinoma	88	0	0	12	0
U2OS*	human	bone	osteosarcoma	80	0	15	5	0
Nontransformed cells after cytokinesis failure								
NIH3T3	mouse	fibroblasts, embryos	normal	0	0	53	31	16
BSC-1	monkey	epithelia, kidney	normal	0	0	8	92	0
BJ	human	fibroblasts, skin	normal	0	0	44	56	0
HMECs	human	mammary gland	normal	0	0	24	52	24

Centrosome numbers were characterized from immunolabeled cells with anti-centrin antibodies.

Metaphase spindles were scored:

Split indicates multipolar spindles with centrioles split apart.

Multipolar indicates multipolar spindle with de-clustered centriole pairs but no splitting of centrioles

Bipolar scattered is bipolar spindle with extra centrosomes scattered along the spindle

* Data from Duensing et al., 2007

** In addition, using serial section electron microscopy of tissue section Lingle and Salisbury (1999) reported that Category III human breast tumors have extra centrioles (11/31 human tumors examined belong to this category) but abnormal mitoses are very rare in vivo.

Abnormal mitotic index (AMI) of Category III tumors is 0.1%

AMI =(abnormal mitotic cells/total mitotic cells)*mitotic index (%)